

partly obscured accretion disk model to explain Shifted broad Balmer emission lines of Active Galactic Nuclei

Xue-Guang Zhang^{1*}, Deborah Dultzin², Ting-Gui Wang³, Guinevere Kaufmann¹

¹Max-Planck Institute für Astrophysik, Karl-Schwarzschild-Strasse 1, 85748 Garching, Germany

²Instituto de Astronomía, Universidad Nacional Autónoma de México, Apdo Postal 70-264, México D. F. 04510, México

³Center for Astrophysics, Department of astronomy and Applied Physics, University of Science and Technology of China, Hefei, Anhui, P.R.China

ABSTRACT

We present a new model to explain the appearance of red/blue-shifted broad low-ionization emission lines, especially emission lines in optical band, which is commonly considered as an indicator of radial motion of the line emitting gas in broad emission line regions (BLRs) of Active Galactic Nuclei (AGN). We show that partly obscured disk-like BLRs of dbp emitters (AGN with double-peak broad low-ionization emission lines) can also successfully produce shifted standard Gaussian broad Balmer emission lines. Then we select eight high quality objects (S/N ≥ 40 at r band) with shifted standard Gaussian broad $H\alpha$ (the shifted velocity larger than $180 \text{ km} \cdot \text{s}^{-1}$) from SDSS DR4. All eight selected objects have visible stellar absorption features in their spectra, except SDSS J1007+1246, which allows us to estimate BH masses through M-sigma relation which has proven to be the most reliable method. We also calculate virial BH masses from continuum luminosity and line width of broad $H\alpha$, assuming broad emission line from "normal" BLRs dominated by virialized motions. We find that the BH masses calculated from M-sigma relation are systematically larger than virial BH masses for the selected objects, even after the correction of internal reddening effects in BLRs. The smaller virial BH masses than BH masses from M-sigma relation for objects with shifted broad emission lines are coincident with what we expect from the partly obscured accretion disk model. Thus, we provide an optional better model to explain the appearance of shifted broad emission lines, especially for those objects with underestimated virial BH masses. Finally, we make predictions about the variation of shifted broad $H\alpha$ with time passage for the two models: Broad $H\alpha$ from "normal" radially moving clouds or broad $H\alpha$ from dbp BLRs in a partly obscured accretion disk.

Key words: Galaxies:Active – Galaxies:Nuclei – quasars:Emission lines

1 INTRODUCTION

There is no way to spatially resolve broad emission line regions (BLRs) of active galactic nuclei (AGN) by direct observation, and no hope of doing so in the foreseeable future. The information about geometry and kinematics/dynamics of BLRs closer to central black hole (BH) can be obtained from study of properties of broad emission lines in observed spectra of AGN. In order to carry out this type of analysis, high signal to noise (S/N ≥ 30) spectra are required. Pioneer work on broad line profiles based on high S/N quasar spectra prior to the SDSS database (Sloan Digital Sky Survey, Adelman-McCarthy et al. 2006) is summarized in Sulentic et al. 2000. An atlas of more than 200 broad $H\alpha$ (some

with higher S/N than data from SDSS) can be found in Marziani et al. (2003). Broad emission lines can be roughly classified into two kinds according to line profiles. Most of them have approximately logarithmic forms, sometimes with slight asymmetry. A small part of them have very complex profiles, such as the double-peaked line profiles. Besides line profiles, variations of broad emission lines, especially variations of strength, have been studied for several decades. From the variations of the broad lines as a response to variations in ionizing continuum emission, the size of BLRs (here 'size' means the distance between central region and BLRs) can be estimated by the reverberation mapping technique (Peterson 1993, 2001) based on pioneer theoretical work by Blandford & McKee (1982). In practice, there are some problems with the application of this technique, e.g. Maoz (1996) has shown that there is not unique one-dimensional transfer

* xueguang@MPA-Garching.MPG.De

function (which can provide some information about geometry of BLRs) for NGC5548. Not to mention the observational effort to monitor the variability of both lines and continuum simultaneously, this has been accomplished for no more than 50 low redshift objects (Collin 2007).

Both from reverberation mapping technique and analysis of high S/N line profiles, we have been able to gather some information on velocity fields of BLRs of AGN. It is widely accepted that the profiles clearly have Doppler origin, and commonly assumed that BLRs clouds are mainly gravitationally dominated by central mass of host galaxy (Gaskell 1996, 1988; Wandel et al. 1999; Peterson & Wandel 1999). However, the basic assumptions can not explain asymmetry in part of broad emission lines. Although there are several possible explanations for the asymmetry, the first and most obvious one is that there is radial motion of BLRs clouds, which has been proved by cross-correlation test (Netzer 1990). Thus asymmetry in broad emission lines indicates that part of emission line clouds in BLRs can be moving away, or perhaps into the central region of AGN. Obviously, if radial flow in BLRs is the dominant component, one shifted logarithmic profile should be expected. Recently, Bonning et al. (2007) proposed to find recoiling black holes system in SDSS through shifted broad emission lines due to radial motion in BLRS, although no convincing evidence to prove recoiling BH in AGN.

Besides normal AGN with broad emission lines having logarithmic form, there is one special kind of AGN, AGN with **Dou**ble-**Pe**aked low-ionization broad emission lines (hereafter, dbp emitters), which have undoubtedly distinct properties of broad emission lines. There are three famous dbp emitters: NGC 1097 (Storchi-Bergmann, Nemmen, et al. 2003, Storchi-Bergmann, Eracleous et al. 1997, Storchi-Bergmann, Eracleous & Halpern 1995, Storchi-Bergmann, Baldwin et al. 1993), Arp102B (Chen et al. 1989a, 1989b, 1997, Halpern et al. 1996, Antonucci et al. 1996, Sulentic et al. 1990) and 3C390.3 (Shapovalova et al. 2001, Gilbert et al. 1999). There are at least two different models proposed to explain observed features of double-peaked broad emission lines. One is the binary black hole model (Begelman et al. 1980, Gaskell 1983). However this model has failed to account for properties of long-term variability and leads to much larger central BH masses than $10^{10}M_{\odot}$ (Eracleous et al. 1997). Thus, we prefer to the other model, the accretion disk model. This model was first proposed by Chen et al. in 1989 (Chen et al. 1989a, 1989b), and then improved from circular accretion disk model to elliptical accretion disk model by Eracleous et al. (1995). The accretion disk model can be successfully applied to reproduce the complex double-peaked broad emission lines and to reproduce the long-term variations of double-peaked emission lines, under the assumption that double-peaked broad emission lines come from disk-like BLRs locating onto central accretion disk.

For dbp emitters, because disk-like BLRs are locating onto accretion disks, one interesting result is that the disk-like BLRs can be partly obscured by dust torus in unified model (Antonucci 1993, Urry & Padovani 1995) and/or by some dust clouds. So, the interesting question is proposed whether broad emission lines of dbp emitters with partly obscured BLRs have similar properties as those of "normal" broad emission lines. In the following section, we develop our model and give some simple but interesting examples of

broad emission lines with standard profiles from partly obscured disk-like BLRs of dbp emitters. In section 3, we try to find some candidates which have shifted standard broad emission lines, but actually are partly-obscured dbp emitters. Section 4 gives the discussion and conclusion. The cosmological parameters $H_0 = 70 \text{ km} \cdot \text{s}^{-1} \text{ Mpc}^{-1}$, $\Omega_{\Lambda} = 0.7$ and $\Omega_m = 0.3$ have been adopted here.

2 THEORETICAL RESULTS FROM PARTLY OBSCURED BLRS OF DBP EMITTERS

The accretion disk model has been proposed and studied by many papers, Circular disk model: Chen et al. 1989, Chen & Halpern 1989, Elliptical disk model: Eracleous et al. 1995, Warped disk model: Bachev 1999, Hartnoll & Blackman 2000, Circular disk with spiral arm model: Hartnoll & Blackman 2002, Karas et al. 2001. Here, we select the elliptical accretion disk model (Eracleous et al. 1995) rather than the other models, because the less parameters of the model can better explain most of the aspects of double-peaked broad emission lines. The elliptical accretion disk model of Eracleous et al. (1995) has 8 free parameters. Five of them are applied to determine the geometrical structure of the disk-like BLRs: the inner radius of disk-like BLRs R_{in} , the outer radius R_{out} , the eccentricity e , the inclination angle i , and the original orientation angle of the BLRs in accretion disk ϕ_0 (the angle between major axis of elliptical disk-like BLRs and direction of projected line-of-sight into accretion disk). Another parameter q is used to determine line emissivity as $f_r \propto r^{-1 \times q}$. Then two other parameters, local broadening velocity dispersion σ_l and amplitude factor k , are used to broaden and strengthen outer broad emission lines. Here, we do not use the parameter k . The normalized flux densities of broad H α from the accretion disk model have a maximum value to 1.

In order to discuss the effects of dust torus on observed broad emission lines from accretion disk model, some parameters of dust torus should be first determined. The size of torus has been determined by reverberation mapping technique applied to the flux variations in the near-infrared and optical bands for some nearby Seyfert 1 galaxies by Suganuma et al. (2006). The mean size of inner side of the torus for these nearby objects is about $\propto (\nu L_{\nu}(V))^{0.5}$, which is about three times larger than the size of BLRs of "normal" AGN as obtained by Kaspi et al. (2005). However, the opening angle of the torus cannot be determined by means of this unique parameter. If we accept that the size of BLRs of normal AGN should be less than the height of the inner side of dust torus, we can roughly determine the opening angle of the torus as about 40 – 50 degrees. Furthermore, the opening angle of torus can be estimated from the number ratio of type 1 to type 2 AGN (Zakamska et al. 2003). We can accept that opening angle of dust torus around 60 degree is a reasonable value. Thus if we adopt 60 degrees as the origin value of inclination angle in accretion disk model, $i = \pi/3$, which leads to the result that some part of disk-like BLRs should be seriously obscured by dust torus.

It is simple to chose the other model parameters to check output broad emission lines from partly obscured accretion disk model. The inner radius is about several hundreds of the gravitational radius, $R_{in} \sim 600R_g$. The outer

radius is about several thousands of the gravitational radius, $R_{out} \sim 4000R_g$. The local broadening velocity is several thousands of kilometers per second, $\sigma_l \sim 3000\text{km} \cdot \text{s}^{-1}$. The slope of the line emissivity can be determined as $f_r \propto r^{-2}$. The eccentricity of the elliptical disk is selected as $e = 0.6$ and the original orientation angle is $\phi_0 \sim \pi/3$. The selected values for the model parameters (except local broadening velocity) above are common values for dbp emitters as shown in Eracleous & Halpern (2003). Here, we select a bit larger local broadening velocity in order to get a clearly fine result as shown in Figure 1. As a simple example of the partly obscured accretion disk model, we consider the case that half of the $\text{H}\alpha$ emitting regions are seriously obscured, i.e., the integral range of orientation angle is not from ϕ_0 to $\phi_0 + 2 \times \pi$, but from $\phi_0 + \pi/2$ to $\phi_0 + 3 \times \pi/2$.

Figure 1 shows some output broad lines with some noise under the partly obscured accretion disk model. We can see that shifted standard gaussian broad $\text{H}\alpha$ emission lines by different input model parameters are produced. The random noise shown in Figure 1 is created assuming that the maximum ratio of noise to flux density is less than 0.07, which is one standard value for SDSS spectra. We can find that different input model parameters lead to different line profiles with different shifted velocities, but can also be best fitted by standard gaussian function. Furthermore, the input model parameter of ϕ_0 should determine if the observed broad $\text{H}\alpha$ is blue-shifted or red-shifted.

Before the end of the section, it is interesting to check effects of the parameter of original orientation angle of partly obscured disk-like BLRs (ϕ_0) on output broad line profile, because the original orientation angle is the only parameter in the elliptical accretion disk model which is varying with the precession of elliptical disk-like BLRs. The precession period should be proportional to $\frac{A \times (1-e^2)}{M_{BH}}$ (A is the length of semi-major axis), for accretion disk around a Schwarzschild black hole, which indicates the precession for inner part of elliptical disk-like BLRs should be about several tens of years, and leads to apparent variations of the parameter of original orientation angle, if central BH masses are large enough and length of semi-major axis is small enough. Thus it is necessary to check the effects of original orientation angle on output broad emission lines under the partly obscured accretion disk model. Actually, in partly obscured accretion disk model, there are some free parameters which can not be determined, such as actual area of obscured disk-like BLRs. Thus, there is so far no clear way to describe detailed effects of the original orientation angle. However, commonly we can simply show that the variation of original orientation angle should have little effects on the output model broad line profiles to some extent under the simple half partly obscured accretion disk model, although the half partly obscured accretion disk model above is oversimplified.

Figure 2 shows some examples of the output broad emission lines with different values of original orientation angle, meanwhile the other disk like parameters are held constant to the ones listed above. There are eighty values of original orientation angle from 0 to $2 \times \pi$ used to produce eighty output broad emission lines, and only 8 of them are shown in Figure 2. It is clear that different orientation angles could lead to standard gaussian line profiles but with different shift velocities. Another interesting result about partly obscured

accretion disk model is that the number of red-shifted model broad line is smaller than the number of blue-shifted model broad line, 25 red-shifted broad lines and 55 blue-shifted model broad lines, because of the elliptical disk-like BLRs with origin point at one focus point of the ellipse. Certainly, the number ratio should depends on the location of the central black hole, near focus point to the observer or far focus point to the observer. Detailed number ratio can be found in Section 3.2. The results shown in Figure 2 indicate that shifted standard gaussian broad emission line is not the case from some special selected original orientation angle.

The results obtained above implies that some AGN (albeit a small number) with shifted broad emission lines with logarithmic profiles may well be dbp emitters with partly obscured disk-like BLRs. There might be different cases for partly obscured BLRs of dbp emitters, those in which a small part of the BLRs are obscured and those where a large part the BLRs are obscured. If the central ring of BLRs is obscured, the expected result is that the peak position should have a small shift velocity, because the rotation velocity of the emission clouds in the outer rings is smaller than that in the inner rings. Furthermore, if the obscured part is not seriously obscured by dust torus, the observed line profile should be seriously asymmetric.

3 OBSERVATIONAL RESULTS FROM SDSS DR4

In this section, we discuss properties of some AGN selected from SDSS DR4 with high qualified shifted standard gaussian broad $\text{H}\alpha$, in order to test our partly obscured accretion disk model. We here focus on objects with higher signal-to-noise ratio than 40 at r band in the main quasars list of SDSS DR4 (Adelman-McCarthy et al. 2006), and with redshift less than 0.37 (in order to ensure the existence of complete broad $\text{H}\alpha$). Then, about 225 objects are firstly selected from SDSS according to criteria about signal-to-noise ratio and redshift. We further check spectra of the selected objects and find that some of them have apparent stellar absorption features, such as absorption lines $\text{MgI}\lambda 5175\text{\AA}$, $\text{CaII}\lambda 3934, 3974\text{\AA}$ and 4000\AA break. Thus we make sure that before we measure line parameters, the stellar components in the observed spectrum are first subtracted.

Before proceeding further, we first give some descriptions about our strict selection criteria. In this paper, we mainly focus on properties of shifted broad balmer emission lines. Thus how to determine whether one broad emission line is shifted is the first question we should find an answer. The common method is to calculate relative shifted value between central wavelengths of broad and narrow emission lines. It is obvious that asymmetry in broad emission lines should have serious effects on determination on central wavelength of broad emission lines. Thus, less asymmetry in high qualified emission lines can lead to better determination of shifted velocity. Besides the convenience to determine shifted velocity, shifted standard gaussian broad emission lines can provide more information about total isotropic radial motions of normal BLRs, if we accept that normal BLRs are locating into so-called ionization cone as described by Unified Model for AGN. In order to confirm observed broad $\text{H}\alpha$ has standard gaussian line profile, objects with high qual-

ity (S/N gt 40) are preferred. In order to confirm the broad emission lines have reliable shifted velocities, objects with apparent shifted velocities (larger than 180 km/s, the SDSS spectral resolution) relative to the center wavelength of narrow H α are selected. Thus number of objects in our final sample should be small, but the small number of objects still provide interesting and enough information about our final conclusion.

An efficient method to subtract the stellar lights is the PCA (Principle Component analysis) method described by Li et al. (2005) and Hao et al. (2005), using the eigenspectra from pure absorption galaxies from SDSS or the eigenspectra from stars in STELIB (Le Borgne et al. 2003), because the method of Principle Component Analysis (PCA) provides a better way to constrict more favorable information from a series of spectra of stars or galaxies into several eigenspectra. Here, we used the method from Hao et al. (2005). The eigenspectra are calculated by KL (Karhunen-Loeve) transformation for about 1500 pure absorption galaxies selected from SDSS DR4. Then, the first eight eigenspectra and the spectra of an A star (which is used to account for young stellar population) selected from STELIB (a library of stellar spectra at $R \sim 2000$, Le Borgne et al. 2003) are used to fit the stellar properties of the observed spectra. After this, rather than a power law, a three-order polynomial function is used to fit the featureless AGN continuum, because the study of composite spectra of AGN shows that the AGN continuum should be best fitted by two power laws with a break at $\sim 5000\text{\AA}$ (Francis et al. 1991, Zheng et al. 1997, Vanden Berk et al. 2001). After the last step, the featureless continuum and the stellar components are obtained based on the Levenberg-Marquardt least-squares minimization method applied for observed spectrum with emission lines masked.

After the subtraction of stellar components and featureless continuum, the line parameters can be measured. Here we focus on the region around H α : broad and narrow components of H α , [NII] $\lambda 6548, 6583\text{\AA}$ and [SII] $\lambda 6716, 6731\text{\AA}$. Then, we measure the line parameters applying gaussian function to each line component. In the procedure, the second moment of broad H α has a lower limit of $400\text{km} \cdot \text{s}^{-1}$, the second moments of narrow emission lines have the same value in velocity space. Once line parameters are measured, objects with shifted velocities larger than 180km/s relative to narrow H α and/or [NII] doublet are selected. Then we carefully check the selected objects by eye to reject those with double-peaked emission lines. We have about 20 objects, of which broad component of H α can be best fitted by one-gaussian function. Then one criterion about χ^2 is finally used to reject some objects. The parameter χ^2 is commonly used to determine whether the model fit by one broad gaussian function is the best choice for broad emission lines limited by $0.5 < \chi^2 < 2.5$, where χ^2 is calculated by $\chi^2 = \frac{\sum(\frac{y-y_{model}}{y_{err}})^2}{dof}$, where dof is degree of freedom. We end up with 8 objects which have shifted standard gaussian broad H α , seven with red-shifted broad H α and one with blue-shifted broad H α . The best fitted results for emission lines around H α are shown in Figure 3. In Table 1, we list the line parameters of the 8 objects.

Before the end of the subsection, we should note that the broad component of H α in SDSS J1649 perhaps is not

so secure, especially from the best fitted results shown in Figure 3. However, through the measured line parameters of broad component of broad H α of SDSS J1649 (listed in Table 1), we also keep the object in our sample according to the criteria above.

3.1 BH Masses and Size of BLRs

The most reliable method to estimate BH masses is based on the stellar velocity dispersion of bulge of the host galaxy, M-sigma relation, first suggested by Ferrarese & Merritt (2000) and Gebhardt et al. (2000), then confirmed by Tremaine et al. (2002) and Merritt & Ferrarese (2001) etc.

$$M_{BH} = 10^{8.13 \pm 0.06} \left(\frac{\sigma}{200\text{km} \cdot \text{s}^{-1}} \right)^{4.02 \pm 0.32} M_{\odot} \quad (1)$$

which indicates strong correlation between BH masses and bulge masses (Häing & Rix 2004, Marconi & Hunt 2003, McLure & Dunlop 2002, Laor 2001, Kormendy 2001, Wandel 1999) etc. Furthermore, More recent results from a larger SDSS sample indicate there is no significant evolution of M-sigma relation by Shen et al. (2008). Besides, the results from observational results, Shankar et al. (2008) theoretically study the evolution of M-sigma relation, and found that from $z \sim 0$ to $z \sim 0.5$, there is no significant evolution of M-sigma relation, which is similar to the result found by Shen et al. (2008). Thus, although the eight objects in our sample have much different redshifts, we think the BH masses from M-sigma relation are still reliable.

However, how to accurately measure stellar velocity dispersion is an open question, because of known problems with the template mismatch. A commonly used method is to select spectra of several kinds of stars (commonly, G and K) as templates, and then broaden the templates by the same velocity to fit stellar features, leaving the contributions from different kinds of stars as free parameters (Rix & White 1992). However, more information about stars included by the templates should lead to more accurate measurement of stellar velocity dispersion. According to the above mentioned method to subtract stellar components, we created a new template rather than several spectra of G or K stars as templates. Thus, we apply the PCA method for all 255 spectra of different kinds of stars in STELIB. Selecting the first several eigenspectra and a three-order polynomial function for the background as templates, the value of stellar velocity dispersion can be measured by the method of minimum χ^2 method applied for the absorption features around MgI $\lambda 5175\text{\AA}$ within rest wavelength range from 5100 \AA to 5300 \AA . The method to measure stellar velocity dispersion is similar to the method to subtract stellar component discussed above. In Figure 4, we show the best fitted result for absorption features near MgI $\lambda 5175\text{\AA}$ for seven objects, except SDSS J1007+1246 because of the lack of MgI $\lambda 5175\text{\AA}$. For SDSS J1007+1246, the line width of narrow emission lines is used as the substitute of stellar velocity dispersion (Nelson & Whittle 1995, Greene & Ho 2005a), $\sigma = 226.37\text{km} \cdot \text{s}^{-1}$. Then BH masses of the eight objects are estimated by M-sigma relation and listed in Table 2. Of course, we check the correlation between line width of narrow emission lines and stellar velocity dispersion for the seven objects, and find the mean value for the ratio of stellar velocity dispersion to line width of narrow emission

lines (the second moment σ , for the standard gaussian line profiles, $FWHM = 2.35 \times \sigma$) to be about 1.06 ± 0.12 , which indicates that the measured stellar velocity dispersions for the seven objects is reasonably accurate. Due to the small number of objects, we do not show the correlation. The values of stellar velocity dispersion and line width of narrow emission lines are listed in Tables 1 and 2.

The BH masses of the eight objects can be also estimated under the assumption of virialization method (Onken et al. 2004, Peterson et al. 2004, Kaspi et al. 2005, Bentz et al. 2006) and listed in Table 2,

$$M_{BH} = 2.36 \times 10^8 \left(\frac{\sigma_B}{3000 \text{km} \cdot \text{s}^{-1}} \right)^2 \left(\frac{L_{5100\text{\AA}}}{10^{44} \text{erg} \cdot \text{s}^{-1}} \right)^{\sim 0.5} M_{\odot} \quad (2)$$

Here, the more recent result about the correlation between size of BLRs and continuum luminosity is used (Bentz et al. 2006). The AGN continuum luminosity is measured from the observed spectrum after the subtraction of stellar components and also listed in Table 2. As we have discussed in Zhang, Dultzin-Hacyan & Wang (2007a), the equation above to estimate virial BH masses of AGN is not accurate for some dwarf AGN with much lower dimensionless accretion rate $m_{H\alpha} = \frac{L_{H\alpha}}{L_{Edd}} < 10^{-5.5}$ (where $L_{H\alpha}$ includes both the broad and narrow components of $H\alpha$), because of the inaccuracy of the empirical relation between continuum luminosity and size of the BLRs. Thus, the virial BH mass of the object SDSS J1649+3613, with $m_{H\alpha} \sim 10^{-6}$ should be smaller than the determined value because R_{BLRs} estimated from continuum luminosity should be smaller than the true size (see also Wang & Zhang 2003).

If the shifted standard gaussian broad $H\alpha$ comes from the partly obscured accretion disk, we should expect that the virial BH masses should be smaller than the more reliable BH masses estimated through stellar velocity dispersions, because of the smaller observed line width and smaller size of BLRs from smaller observed continuum luminosity than intrinsic ones from partly obscured accretion disk model. Figure 5 shows the comparison of the two kinds of BH masses of the eight objects. From the figure, we can see that BH masses estimated through M-sigma relation are systemically larger than virial BH masses, $\langle \frac{M_{BH}(\sigma)}{M_{BH}(\text{virial})} \rangle \sim 68$ for all the eight object (If the object SDSS J1649 is rejected, the mean ratio of the two kinds of BH masses is 16). The result strongly indicates that the partly obscured accretion disk model is preferred to the objects in our sample, especially SDSS J1044, SDSS J1457 and SDSS J1715.

It is obvious that we do not consider effects from internal reddening on results above. Commonly, effects of internal reddening can be corrected through balmer decrements from broad balmer emission lines, especially flux ratio of broad $H\alpha$ to broad $H\beta$, assuming internal balmer decrement for broad $H\alpha$ to broad $H\beta$ is about 3.1. The flux ratios of broad $H\alpha$ to broad $H\beta$ are listed in Table 2 for the eight objects. According to observed flux ratios of $H\alpha$ to $H\beta$, internal luminosity of broad and $H\alpha$ are determined, after the correction of internal reddening effects. Then according to the correlation between continuum luminosity and line luminosity for a sample of quasars (Greene & Ho 2005b), internal AGN continuum luminosity is estimated for each object in our sample. In other words, after the correction of internal reddening effects, we ensure that flux ratio of $H\alpha$ to $H\beta$ is

3.1, and the correlation luminosity of $H\alpha$ and continuum luminosity obeys the one found in Greene & Ho (2005b). According to the AGN continuum luminosity after the correction of internal reddening effects, the virial BH masses are re-measured by Equation (2), and re-shown in Figure 6. We can clearly see that the effects of internal reddening cannot change the result: BH masses estimated through stellar velocity are systemically larger than virial BH masses.

If we assume that the broad $H\alpha$ of each object in our sample is emitted from "normal" BLRs, its distance to the BH (its size) can be estimated from the continuum luminosity after the correction of internal reddening (Bentz et al. 2006), $R_{BLRs} \propto L_{5100\text{\AA}}^{\sim 0.5}$, except for SDSS J1649 which has much smaller dimensionless accretion rate $m_{H\alpha} < -5.5$ (Zhang, Dultzin-Hacyan & Wang 2007a). The estimated size of BLRs of each object is listed in Table 2. If the shifted broad $H\alpha$ are interpreted by emitting regions dominated by radial motions, it is clear that radial motions should lead to change of size of BLRs, and then lead to change of line width. There are 7 out of 8 objects show red-shifted broad profiles. The red-shifted velocity indicates the direction of the radial flows points to the central black hole. The inferred "infalling times" for such emission clouds were estimated and are listed in Table 2. The implication is the following: If the shift of broad $H\alpha$ is due to infalling emission clouds, after several years the broad line emission clouds would be accreted into the central accretion disk or into the central black hole, and thus the observed broad $H\alpha$ should have complex line profiles rather standard gaussian profiles.

Finally, we want to point out that the smaller line width of broad $H\alpha$ for objects in our sample is about 30\AA (second moment). It is necessary to check whether the partly obscured disk model can reproduce the outward shifted standard gaussian broad $H\alpha$ with small line width. If we select the following model parameters: $R_{in} \sim 6286R_g$, $R_{out} \sim 45000R_g$, $i = 60^\circ$, $f_r \propto r^{-1.5}$, $e = 0.8$, $\sigma_l \sim 1550 \text{km} \cdot \text{s}^{-1}$ and $\phi_0 \sim 55^\circ$, the outward gaussian broad $H\alpha$ line profile of SDSS J1715+5935 can be nearly reproduced with a second moment of 38.28\AA and with center wavelength at 6577.92\AA . For this we have to assume that half of the disk-like BLRs in accretion disk are obscured. This is, however, a very particular assumption to explain a particular case. By changing of the input model parameters, outward broad line with different line width and different shifted velocity can be obtained. However, we should notice that this is a simple model, where we assume that half of the broad dbp clouds are heavily obscured by the dust torus. Probably the actual case is much complex. Thus here we do not give specific model parameters for the objects in our sample, our main objective is to show that partly obscured dbp BLRs can lead to shifted broad lines with normal form.

3.2 Number Ratio of Objects with Red-Shifted Velocities to Objects with Blue-Shifted Velocities

In this subsection, we will discuss the number ratio of objects with red-shifted observed broad standard gaussian $H\alpha$ to objects with blue-shifted observed broad standard gaussian $H\alpha$, N_{rb} , under the partly obscured accretion disk model, which will provide more evidence for the model.

As what we have done in section 2, we can find that under the partly obscured accretion disk model, the value of $N_{r,b}$ is about $\frac{25}{55}$. It is clear that the value should depend on the location of central black hole in the accretion disk model, if the radius of one particle is described by $r = \frac{r_* (1+e)}{1+e \times \cos(\phi - \phi_0)}$ (where r_* and e are the pericenter distance and eccentricity of one elliptical ring), rather than by $r = \frac{r_* (1+e)}{1-e \times \cos(\phi - \phi_0)}$, (in other words, the new orientation angle ϕ^* is described as $\phi^* = \phi + \pi$), the value of $N_{r,b}$ should be $\frac{55}{25}$. Especially, if the eccentricity is around zero, i.e., circular disk-like BLRs, it is obvious that the number ratio of $N_{r,b}$ should be 1. Thus the number ratio from the partly obscured accretion disk model is around 1.

However, there is only one object with blue shifted standard broad gaussian H α . Perhaps the weird number ratio is due to the strict selection criteria. Figure 7 shows the distribution of shifted velocities ($w_0(H\alpha_B) - w_0(H\alpha_N)$) of all broad line AGN with reliable standard gaussian broad H α . The value of $N_{r,b}$ is about 1.02 for the 1672 selected broad line AGN. Simply procedure to select the objects as follows. The emission lines around H α are fitted twice. Firstly, each gaussian function is applied to each emission line, broad and narrow emission lines, for all the 8668 QSOs in SDSS DR6. Then the parameter of χ_1^2 is measured. Secondly, double broad gaussian functions are applied to broad H α , with measured parameter χ_2^2 . Then only the objects with similar values of $\chi_1^2 < 2$ and $\chi_2^2 < 2$, $\chi_1^2 - \chi_2^2 \leq 0.1$, are selected. The similar values of χ_1^2 and χ_2^2 mean that the double gaussian functions for broad H α is meaningless. Thus the weird number ratio for the objects listed in Table 1 and in Table 2 is due to the strict selection criteria, not a intrinsic phenomenon.

Furthermore, we check the correlation between virial BH masses estimated from equation (2) and BH masses from M-sigma relation in equation (1) for the 216 objects with reliable measured stellar velocities through absorption features around MgI λ 5175Å, and with shifted velocities larger than 180 km/s. Figure 6 shows the results. We can find what we have expected from partly obscured accretion disk model: the BH masses from M-sigma relation are one magnitude higher than the virial BH masses for the objects with shifted velocities larger than 180km/s, $\langle \frac{M_{BH}(\sigma)}{M_{BH}(virial)} \rangle \sim 17$.

To sum up, if the selection criteria are not so strict, the number ratio of $N_{r,b}$ should be around 1, as shown in Figure 7. However, for low quality SDSS spectra with smaller S/N, it is difficult to confirm the observed broad H α have standard gaussian profiles, because of the strong noise in the spectra. Certainly, it is reasonable to obtain some statistical results through the large sample of objects with low quality, as shown in Figure 6. Certainly, the radial motions in BLRs for shifted broad emission lines are not rejected, because some objects have coincident virial BH masses and BH masses from M-sigma relation. However we provide an optional model to explain the appearance of shifted broad emission lines, especially for those objects with underestimated virial BH masses. Certainly, there are some observed evidence which can be used to determine which model, the partly obscured accretion disk model or radial motions in BLRs model, should be preferred for AGN with underestimated virial BH masses, as discussed in the following section.

4 DISCUSSIONS

In this paper we present a new and interesting model to explain the appearance of shifted broad emission lines, besides the radial motions of broad emission line clouds in BLRs. The scenario considers the partly obscuration of disk-like BLRs in the accretion disk of dbp emitters. From the shift velocity of broad line, we cannot determine velocity field of the broad line clouds in BLRs. We cannot firmly discard radial motions into the Black Hole or away from it. But we can predict that if the shifted standard gaussian broad lines are emitted from a "normal" BLRs in an ionization cone, we expect the line width to change with time passage (BLRs near the central Black Hole produce broader emission lines), but the line profile should keep its form. As shown in Table 2, the infalling times for several objects are only around ten years, thus it should be possible to determine whether radial motions are dominant in these objects by observational spectroscopic monitoring. On the other hand if our model of partly obscured BLRs of dbp emitters is the correct one, we expect that the shapes of the line profiles for some special cases will change with time passage, especially the peak intensity, if the precession of elliptical disk-like BLRs is not so longer than several hundreds of years. Because we only have single epoch spectra, it is difficult to determine the model parameters for the objects in our sample. Thus here we do not give the precession period of BLRs into accretion disk for dbp emitters, and can not give a clear time prediction for observing the change in line profiles. Thus the long-period monitoring of these objects is an interesting observational project to confirm our model.

Furthermore, besides the shifted standard broad gaussian emission lines, it is interesting to discuss the objects with asymmetric broad emission lines. Commonly, the asymmetry is considered as the effects of radial motions in part of normal BLRs. However, the asymmetric non-virialized components in broad emission lines should lead to overestimated virial BH masses. Thus it is clear that there are obviously different characters of virial BH masses estimated from the radial motions in BLRs model and from the partly obscured accretion disk model. The radial motions in BLRs always indicates overestimated virial BH masses, however, partly obscured accretion disk model leads to underestimated virial BH masses.

Finally, we can resume our conclusions as follows: We present a model to explain the appearance of shifted Balmer broad emission lines which does not need to involve radial motions dominating the emission line clouds. We show that partly obscured BLRs of dbp emitters can also produce shifted standard Gaussian broad emission lines. Then we select eight high quality objects (with S/N at r band larger than 40) with shifted broad H α (the shifted velocity larger than 180 km \cdot s $^{-1}$) from SDSS DR4 (seven of them have observable stellar absorption features). Reliable BH masses determined using stellar velocity dispersions result systematically larger than virial BH masses estimated by line width of broad H α and continuum luminosity. We further estimate the size of BLRs for the objects from continuum luminosity and show that internal reddening has no important influence on our final results. Finally, we make predictions about the variation of shifted broad H α with time passage for the two

models: Broad H α from "normal" radially moving clouds or broad H α from dbp BLRs in a partly obscured accretion disk.

ACKNOWLEDGEMENTS

ZXG gratefully acknowledges the postdoctoral scholarships offered by Max-Planck Institute für Astrophysik. D. D acknowledges support from grant IN100507 from DGAPA, UNAM. This paper has made use of the data from the SDSS projects. Funding for the creation and the distribution of the SDSS Archive has been provided by the Alfred P. Sloan Foundation, the Participating Institutions, the National Aeronautics and Space Administration, the National Science Foundation, the U.S. Department of Energy, the Japanese Monbukagakusho, and the Max Planck Society. The SDSS is managed by the Astrophysical Research Consortium (ARC) for the Participating Institutions. The Participating Institutions are The University of Chicago, Fermilab, the Institute for Advanced Study, the Japan Participation Group, The Johns Hopkins University, Los Alamos National Laboratory, the Max-Planck-Institute for Astronomy (MPIA), the Max-Planck-Institute for Astrophysics (MPA), New Mexico State University, Princeton University, the United States Naval Observatory, and the University of Washington.

REFERENCES

- Adelman-McCarthy J. K., et al., 2006, ApJS, 162, 38
 Antonucci R., 1993, ARA & A, 31, 473
 Antonucci, R., Hurt, T. & Agol, E., 1996, ApJ, 456, 25
 Bachev R., 1999, A&A, 348, 71
 Begelman M. C., Blandford R. D. & Rees M. J., 1980, Nature, 287, 307
 Bentz M. C., Peterson B. M., Pogge R. W., Vestergaard M., Onken C. A., 2006, ApJ, 644, 133
 Blandford R. D. & McKee C. F., 1982, ApJ, 255, 419
 Bonning E. W., Shields G. A., Salviander S., 2007, ApJ, 666, L13
 Chen K. Y. & Halpern J. P., 1989, ApJ, 344, 115
 Chen K. Y., Halpern J. P. & Filippenko A. V., 1989, ApJ, 339, 742
 Chen K. Y., Halpern J. P. & Titarchuk L. G., 1997, ApJ, 483, 194
 Collin S., Black Holes from Stars to Galaxies – Across the Range of Masses. Edited by V. Karas and G. Matt. Proceedings of IAU Symposium #238, held 21-25 August, 2006 in Prague, Czech Republic. Cambridge, UK: Cambridge University Press, 2007., pp.111-116
 Eracleous M., Livio M., Halpern J. P., Storchi-Bergmann T., 1995, ApJ, 438, 610
 Eracleous M., Halpern J. P., Gilbert A. M., Newman J. A. & Filippenko A. V., 1997, ApJ, 490, 216
 Eracleous M. & Halpern J. P., 2003, ApJ, 599, 886
 Ferrarese L., Merritt D., 2000, ApJ, 539, L9
 Francis P. J., Hewett P. C., Foltz C. B., et al., 1991, ApJ, 373, 465
 Gaskell C. M., 1983, Nature, 304, 212
 Gaskell C. M., 1988, ApJ, 325, 114
 Gaskell C. M., 1996, ApJ, 464, L107
 Gebhardt K., et al., 2000, ApJ, 539, L13
 Gilbert A. M., Eracleous M., Filippenko A. V. & Halpern J. P., 1999, AAS, 194, 7302
 Greene J. E. & Ho L. C., 2005a, ApJ, 627, 721
 Greene J. E. & Ho L. C., 2005b, ApJ, 630, 122
 Halpern J. P., Eracleous M., Filippenko A. V. & Chen K. Y., 1996, ApJ, 464, 704
 Hao L., et al., 2005, AJ, 129, 1783
 Häring, N., Rix, Hans-Walter, 2004, ApJ, 640, L89
 Hartnoll S. A. & Blackman E. G., 2000, MNRAS, 317, 880
 Hartnoll S. A. & Blackman E. G., 2002, MNRAS, 332, L1
 Karas V., Martocchia A. & Subr L., 2001, PASJ, 53, 189
 Kaspi S., Maoz D., Netzer H., Peterson B. M., et al., 2005, ApJ, 629, 61
 Kormendy J., 2001, in Galaxy Disks and Disk Galaxies, proceeding of a conference held in Rome, Italy, June 12-16, 2000 at the Pontifical Gregorian University and sponsored by the Vatican Observatory. ASP Conference Series, Vol. 230. Edited by Jose G. Funes, S. J. and Enrico Maria Corsini. San Francisco: Astronomical Society of the Pacific. ISBN: 1-58381-063-3, 2001, pp. 247-256
 Laor A., 2001, ApJ, 533, 677
 Le Borgne J. F., et al., 2003, A&A, 402, 433
 Li C., Wang T. G., Zhou H. Y., Dong X. B., Chen F. Z., 2005, AJ, 129, 669
 Maoz D., 1996, Emission Lines in Active Galaxies: New Methods and Techniques; IAU Colloquium 159. Astronomical Society of the Pacific Conference Series 113; Proceedings of a meeting held in Shanghai; People's Republic of China; 17-20 June 1996; San Francisco: edited by Bradley M. Peterson, Fu-zhen Cheng, and Andrew S. Wilson., p.138
 Marziani P., Sulentic J. W., Zamanov R., Calvani M., Dultzin-Hacyan D., Bachev R., Zwitter T., 2003, ApJS, 145, 199
 Marconi A. & Hunt L. K., 2003, ApJ, 589, L21
 McLure R. J. & Dunlop J. S., 2002, MNRAS, 331, 795
 Merritt D., Ferrarese L., 2001, ApJ, 547, 140
 Nelson C. H. & Whittle M., 1995, ApJS, 99, 67
 Netzer H., 1990, 20. Saas-Fee Advanced Course of the Swiss Society for Astrophysics and Astronomy: Active galactic nuclei, p. 57 - 160
 Onken C. A., Ferrarese L., Merritt D., Peterson B. M., Pogge R. W., Vestergaard M., Wandel A., 2004, ApJ, 615, 645
 Peterson B. M., 1993, PASP, 105, 247
 Peterson B. M. & Wandel A., 1999, ApJ, 521, L95
 Peterson B. M., 2001, in Advanced Lectures on the Starburst AGN Connection, ed. I. Aretxaga, D. Kunth & R. Mujica (Singapore: World Scientific), p. 3, astro-ph/0109495
 Peterson B. M., et al., 2004, ApJ, 613, 682
 Rix H.-W., White S. D. M., 1992, MNRAS, 254, 389
 Shankar F., Bernardi M., Haiman Z., 2008, astro-ph/0806.3459
 Shapovalova A. I., Burenkov A. N., Carrasco L., et al., 2001, A&A, 376, 775
 Shen J., Vanden Berk D. E., Schneider D. P., Hall P. B., 2008, ApJ, 135, 928
 Storchi-Bergmann T., Baldwin J. A. & Wilson A. S., 1993, ApJ, 410, L11
 Storchi-Bergmann T., Eracleous M., Livio M., et al., 1995, ApJ, 443, 617
 Storchi-Bergmann T., Eracleous M., Ruiz M. T., et al., 1997, ApJ, 489, 87
 Storchi-Bergmann T., Nemmen da S. R., Eracleous M., Halpern J. P., et al., 1997, ApJ, 489, 8
 Suganuma M., Yoshii Y., Kobayashi Y., Minezaki T., Enya K., Tomita H., Aoki T., Koshida S., Peterson B. A., ApJ, 2006, 639, 46
 Sulentic J. W., Zheng W., Calvani M. & Marziani P., 1990, ApJ, 355, 15
 Sulentic J. W., Marziani P., Dultzin-Hacyan D., 2000, ARA&A, 38, 521
 Tremaine S., Gebhardt K., Bender R., Bower G., et al., 2002, ApJ, 574, 740

Table 1. Parameters of emission lines

id	Name	z	$w_{0,N}$ (\AA)	σ_N (\AA)	flux _N	$w_{0,B}$ (\AA)	σ_B (\AA)	flux _B	χ^2
0	J093943.74+560230.4	0.116	6566.70±0.23	3.94±0.31	103.059±10.93	6557.62±0.18	44.50±0.19	7321.52±34.17	1.79
1	J100726.10+124856.2	0.240	6562.47±0.17	4.95±0.21	827.151±31.22	6576.65±0.47	65.41±0.66	14279.4±145.2	0.83
2	J102044.43+013048.4	0.096	6565.87±0.02	1.77±0.02	310.504±4.708	6574.76±0.54	49.74±0.64	1728.50±23.29	1.12
3	J104451.73+063548.6	0.027	6565.12±0.03	3.86±0.04	1522.16±34.03	6570.33±0.39	18.49±0.28	2251.47±68.52	1.99
4	J145706.79+494008.4	0.013	6565.75±0.04	2.41±0.04	1902.73±40.37	6570.76±0.21	21.15±0.19	6961.25±79.99	1.12
5	J164909.58+361325.8	0.030	6566.17±0.09	6.31±0.12	1626.77±50.02	6571.28±1.04	26.12±1.68	1026.26±105.3	1.46
6	J171322.58+325628.0	0.101	6565.42±0.07	4.21±0.09	461.218±9.292	6571.57±0.33	43.90±0.45	2594.12±24.25	1.01
7	J171550.49+593548.7	0.065	6565.48±0.07	3.68±0.08	202.362±5.110	6577.68±0.24	37.16±0.28	1879.38±14.48	2.18

Notes:–

First column is the name of each object in the format of 'Jhhmss.ss±ddmss.s', second column is the redshift. Third to fifth columns list the line parameters of narrow H α , center wavelength in unit of \AA , line width in unit of \AA and flux in unit of $10^{-17}\text{erg} \cdot \text{s}^{-1} \cdot \text{cm}^{-2}$ of narrow H α . Then the line parameters of broad H α are listed in next three columns, center wavelength in unit of \AA , line width in unit of \AA and flux in unit of $10^{-17}\text{erg} \cdot \text{s}^{-1} \cdot \text{cm}^{-2}$ of broad H α . The value of χ^2 is listed in the last column.

Table 2. Parameters of emission lines

id	name	σ	$m_{H\alpha}$	BD	$L_{5100\text{\AA}}$	$M_{BH}(\sigma)$	$M_{BH}(V)$	R_{BLRs}	t_{in}
0	J093943.74+560230.4	165.52±26.62	-3.5	3.67	43.85	7.79	7.96	20.24	
1	J100726.10+124856.2	226.37±7.17	-3.0	5.14	44.94	8.34	8.89	80.49	102.1
2	J102044.43+013048.4	137.64±15.36	-3.9	3.89	43.23	7.47	7.71	9.23	18.6
3	J104451.73+063548.6	148.48±11.53	-4.9	15.13	43.29	7.61	6.88	9.96	34.3
4	J145706.79+494008.4	140.43±12.26	-5.1	4.14	42.29	7.51	6.45	2.81	10.1
5	J164909.58+361325.8	264.23±15.46	-5.9	12.68	42.98	8.61	6.82*	6.72	23.7
6	J171322.58+325628.0	171.56±20.50	-4.1	3.64	43.38	7.86	7.68	11.15	32.7
7	J171550.49+593548.7	151.30±16.15	-4.4	4.31	43.01	7.64	7.33	6.98	10.3

Notes:–

The id number and name for each object is listed in the first and second column. Third column gives the value of stellar velocity dispersion in unit of $\text{km} \cdot \text{s}^{-1}$. Forth column is the dimensionless accretion rate by luminosity of H α before the correction of internal reddening for BLRs $m_{H\alpha}$. The flux ratio of broad H α to broad H β is listed in Column V. Then the internal logarithmic continuum luminosity at 5100 \AA in unit of $\text{erg} \cdot \text{s}^{-1}$ is shown in the next column, after consideration of the effects of internal reddening. Column VII - VIII are the two kinds of logarithmic BH masses in unit of M_{\odot} , $M_{BH}(\sigma)$ is estimated from stellar velocity dispersion, $M_{BH}(V)$ is the virial BH masses through line width of broad H α and continuum luminosity listed in Column VI. For SDSS J1649, the listed virial BH mass in the table is the low-limited one. The last two columns are the size of BLRs in unit of light-days estimated by the continuum luminosity listed in Column VI and the infalling time in unit of years.

- Urry C. M., Padovani P., 1995, PASP, 107, 803
Vanden Berk, D. E., et al., 2001, AJ, 122, 549
Wandel A., 1999, ApJ, 519, L39
Wandel A., Peterson B. M. & Malkan M. A., 1999, ApJ, 526, 579
Wang T. G. & Zhang X. G., 2003, MNRAS, 340, 793
Zakamska et al., 2003, AJ, 126, 2125
Zhang X. G., Dultzin-Hacyan D. & Wang T. G., 2007, MNRAS, 374, 691
Zheng W., Kriss G. A., Telfer R. C., Grimes J. P., Davidsen A. F., 1997, ApJ, 475, 469

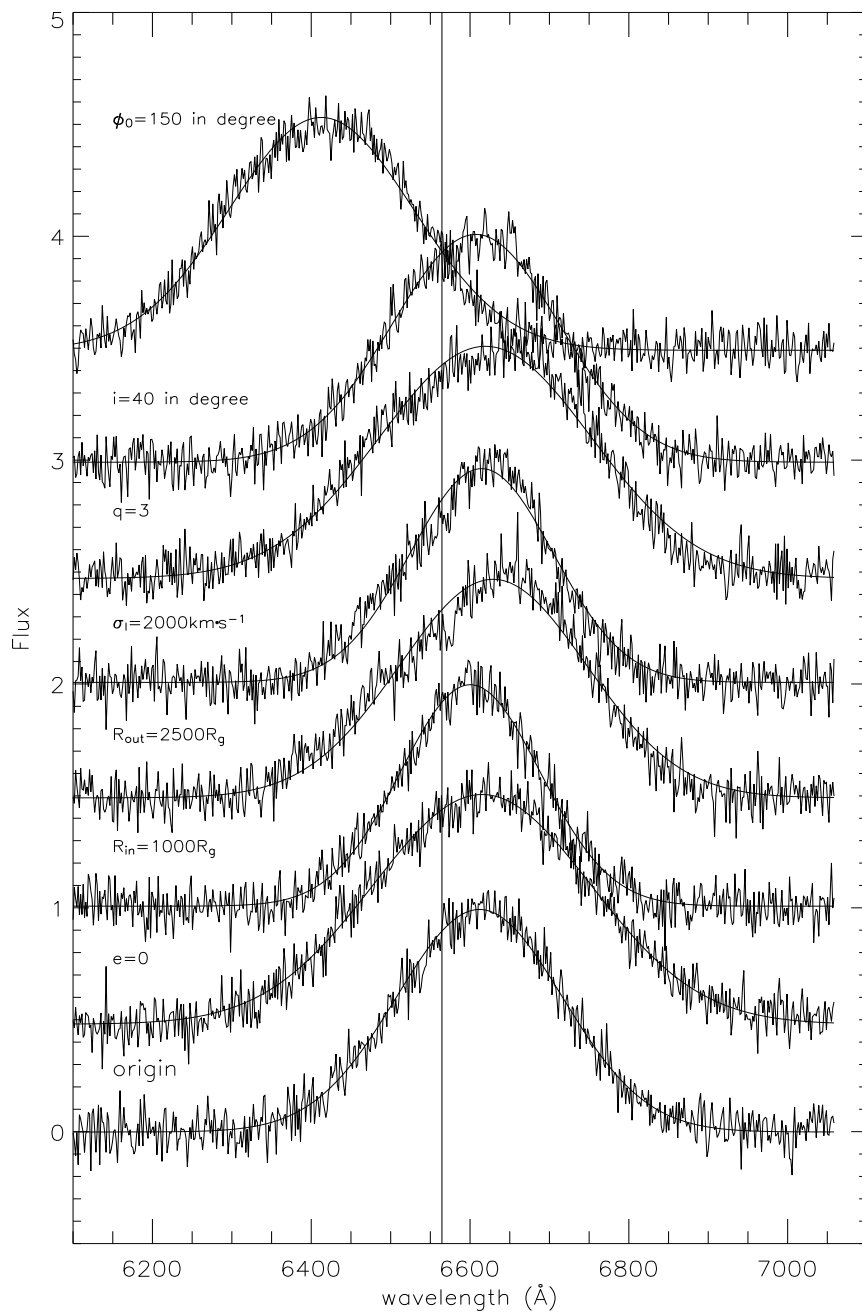


Figure 1. The created examples for broad H α by the partly obscured elliptical accretion disk model. The thin line represents the created broad line by model. Solid line represents the best fitted result by gaussian function. The vertical line marks the position of the center wavelength of normal broad H α in rest wavelength. For each created broad H α , the different input parameter is listed in the figure.

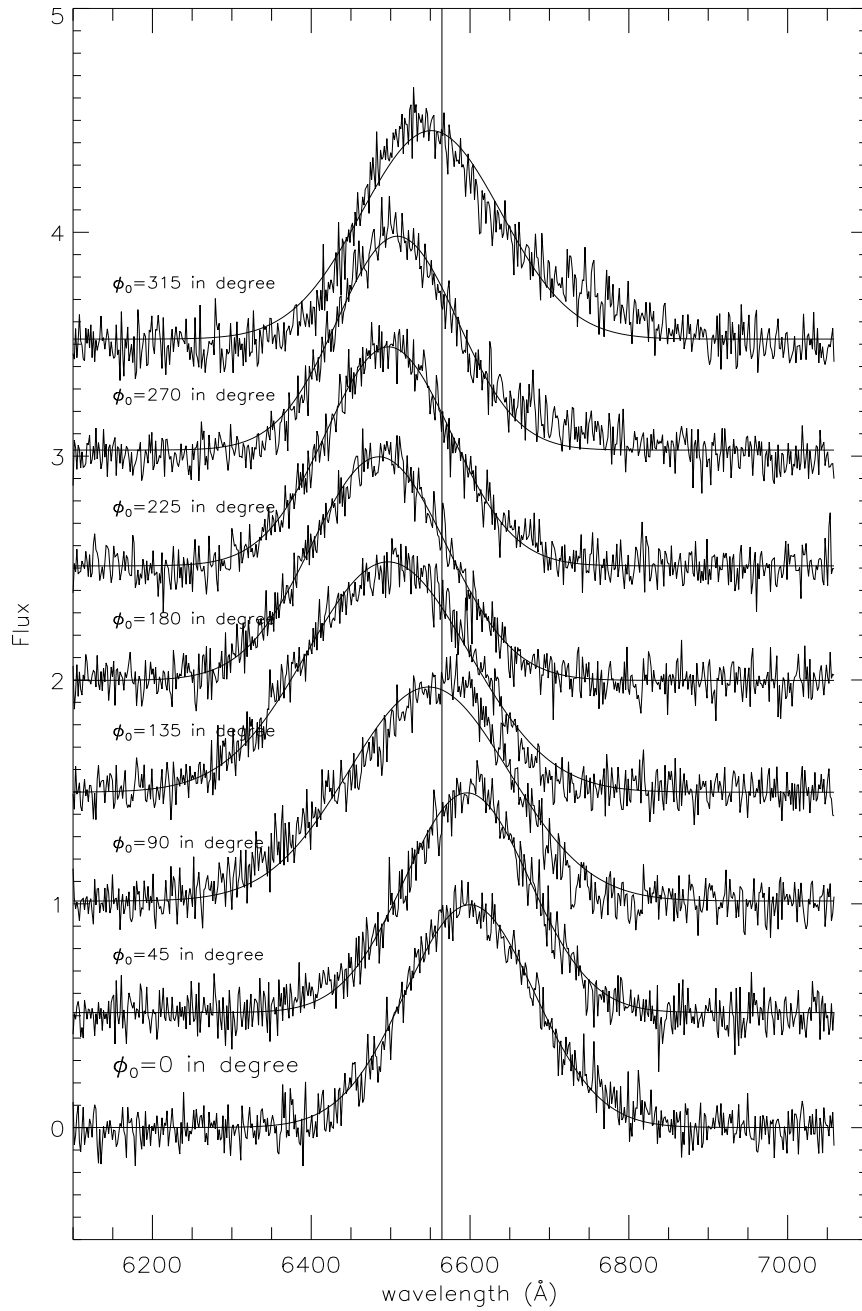


Figure 2. The created example for broad H α by the partly obscured elliptical accretion disk model. The thin line represents the created broad line by model. Solid line represents the best fitted result by gaussian function. The vertical line marks the position of the center wavelength of normal broad H α in rest wavelength. For each created broad H α , the different input parameter of orientation angle is listed in the figure, meanwhile the other parameters are held to constant to the values listed in text.

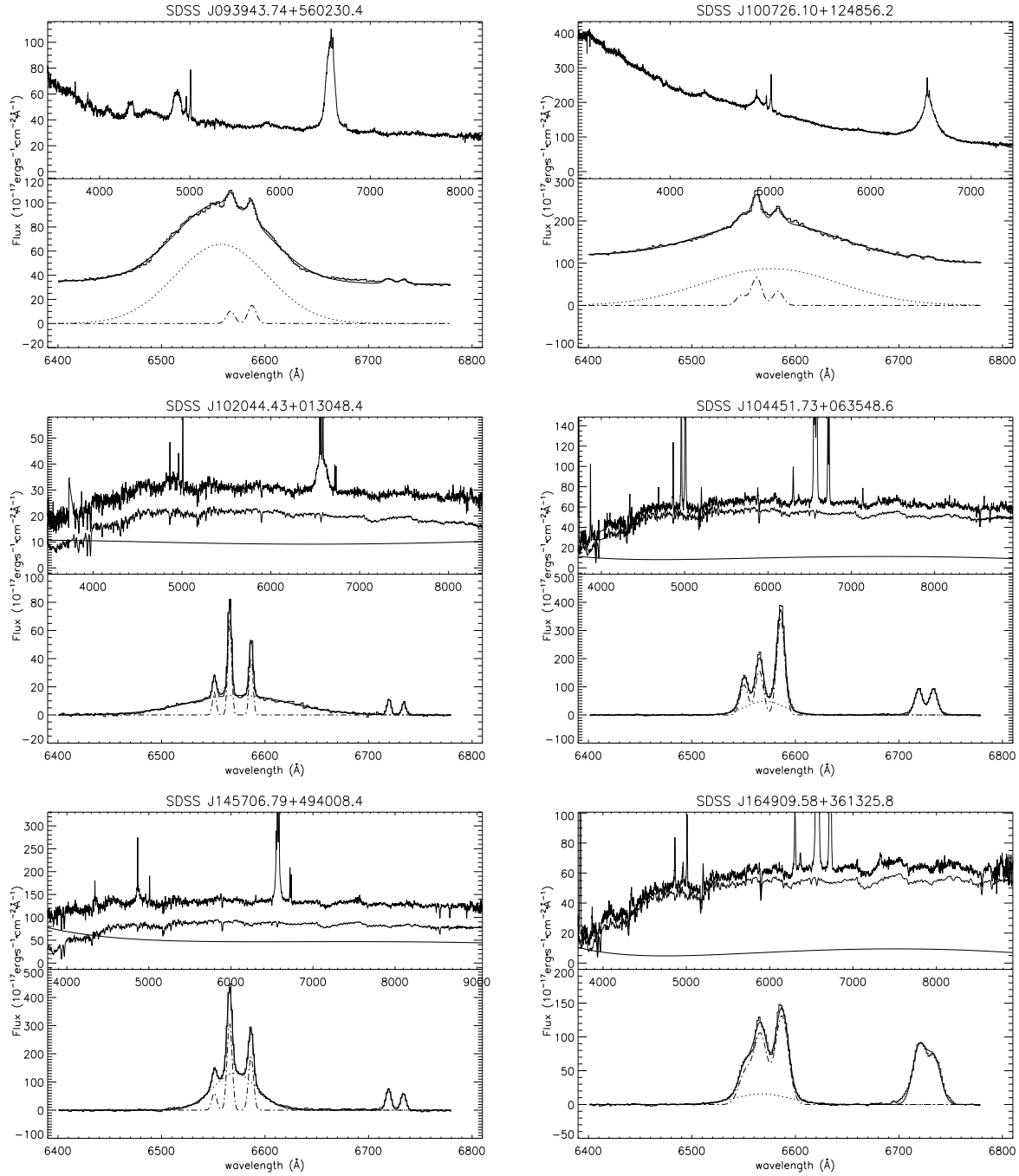


Figure 3. The best fitted results for emission lines around $H\alpha$ are shown in bottom panel for each object. In the panel, thin solid line represents the observed spectrum, thick solid is for the best fitted results, dotted line is for the standard gaussian broad $H\alpha$, dot-dashed line represents the narrow components of $H\alpha$ and $[NII]\lambda 6548, 6583\text{\AA}$. In top panel for each object, the observed spectrum is shown. If there is apparent stellar features, the features and featureless continuum emission are also shown in the panel. If there is no stellar features, only the observed spectrum is shown in the panel. The best fitted

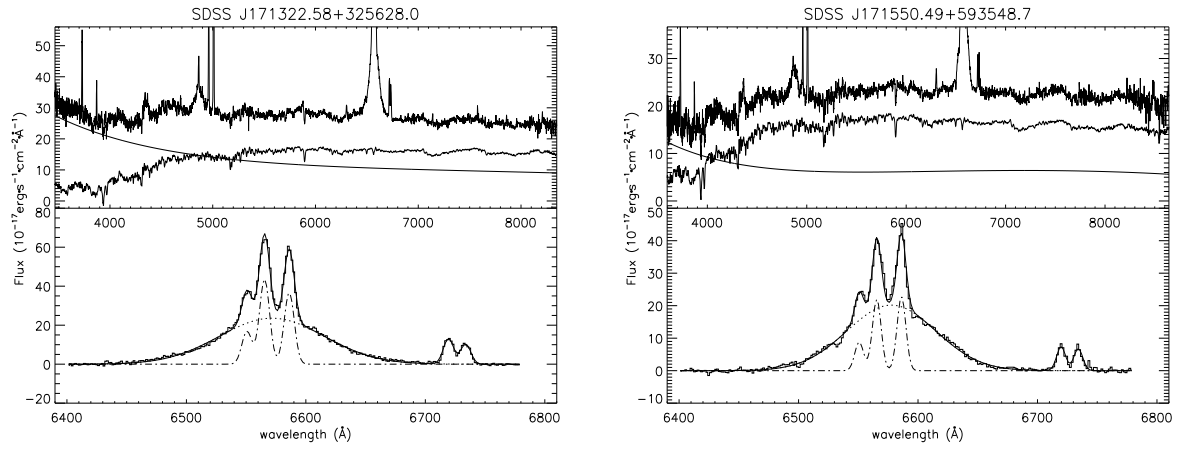


Figure 3. – Continued.

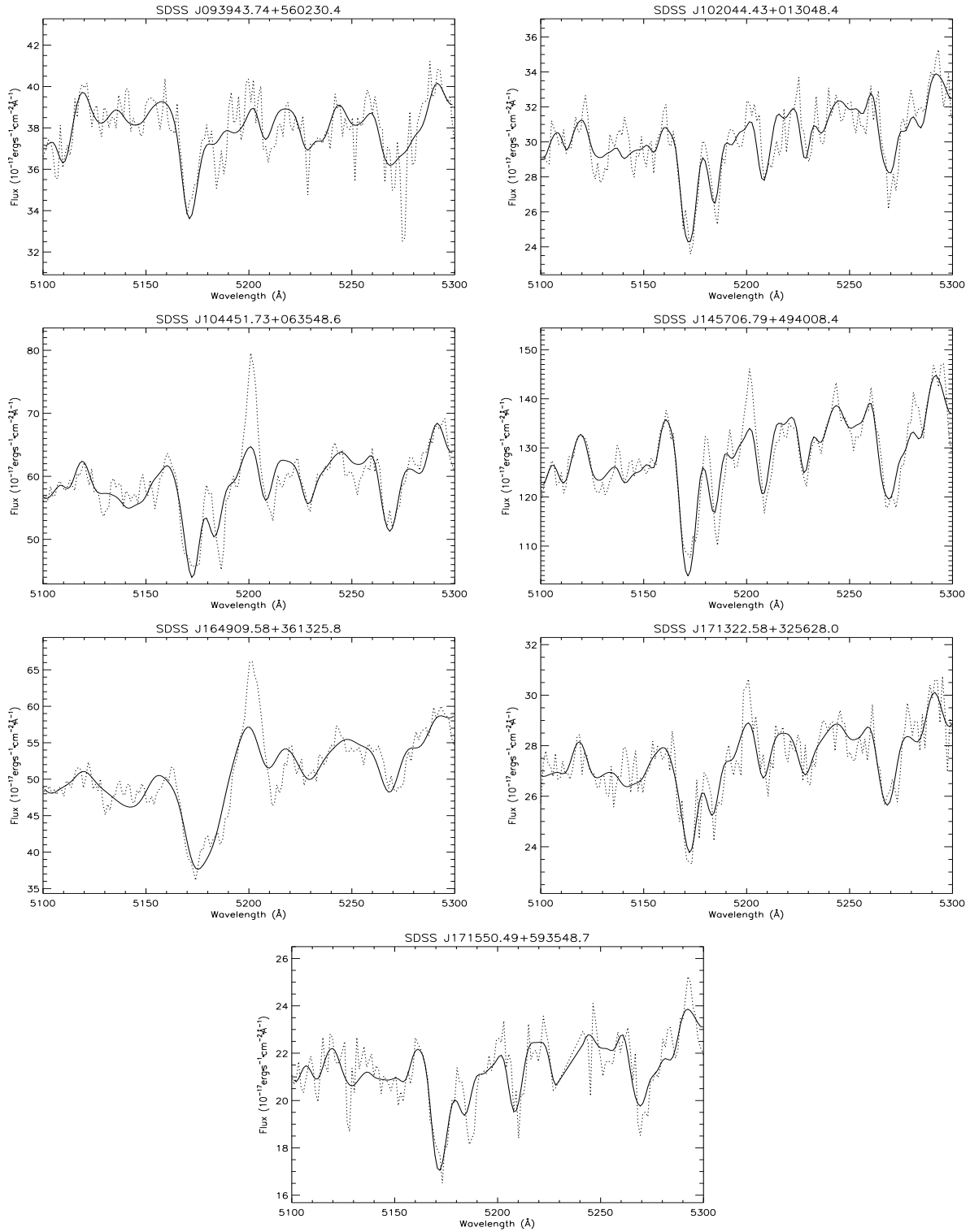


Figure 4. The best fitted results for absorption features near $\text{MgI}\lambda 5175\text{Å}$. Dotted line represents the observed spectrum, solid line is for the best fitted results.

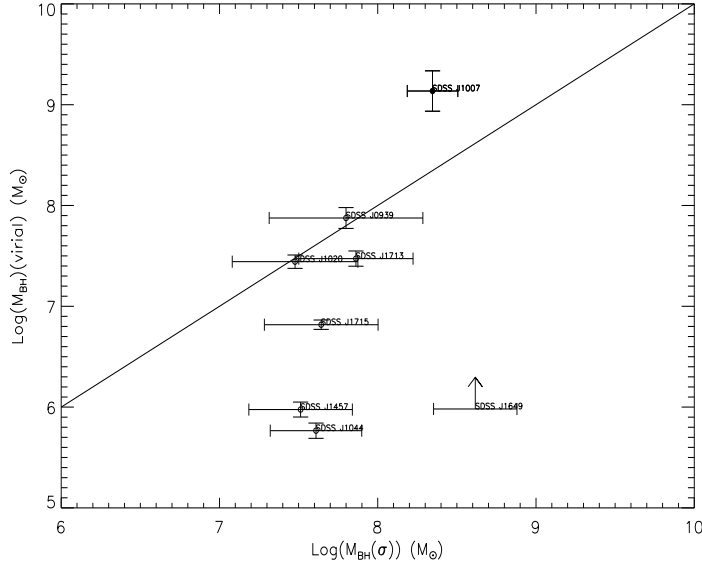


Figure 5. The correlation between two kinds of BH masses, $M_{BH}(\sigma)$ is estimated through stellar velocity dispersion, $M_{BH}(virial)$ is estimated by line width of broad $H\alpha$ and continuum luminosity. Solid circle represents the object of SDSS J1007, of which the stellar velocity dispersion is substituted by line width of narrow emission lines. The upward arrow for object SDSS J1649 indicates that actual virial BH mass should be larger than the one. Solid line represents $M_{BH}(\sigma) = M_{BH}(virial)$.

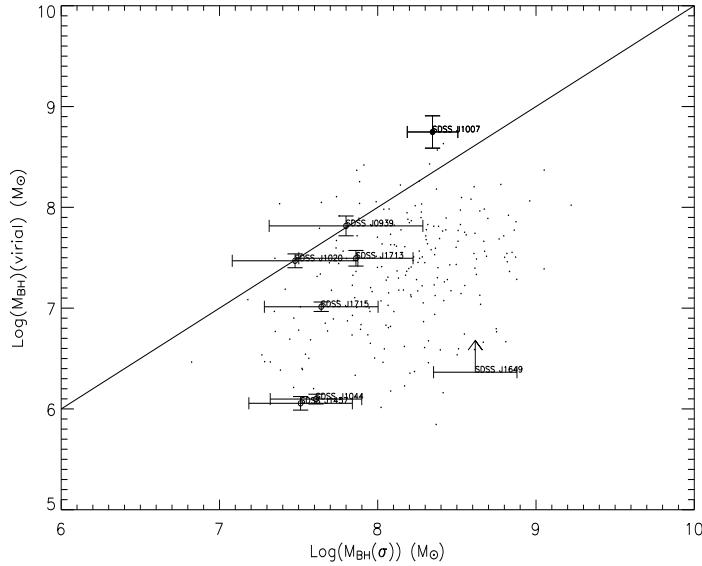


Figure 6. The correlation between two kinds of BH masses after the correction of internal reddening effects, $M_{BH}(\sigma)$ is estimated through stellar velocity dispersion, $M_{BH}(virial)$ is estimated by line width of broad $H\alpha$ and continuum luminosity. Solid circle represents the object of SDSS J1007, of which the stellar velocity dispersion is substituted by line width of narrow emission lines. The upward arrow for object SDSS J1649 indicates that actual virial BH mass should be larger than the one. Solid line represents $M_{BH}(\sigma) = M_{BH}(virial)$. The solid small dots are the objects selected from DR6 with shifted velocities larger than 180km/s.

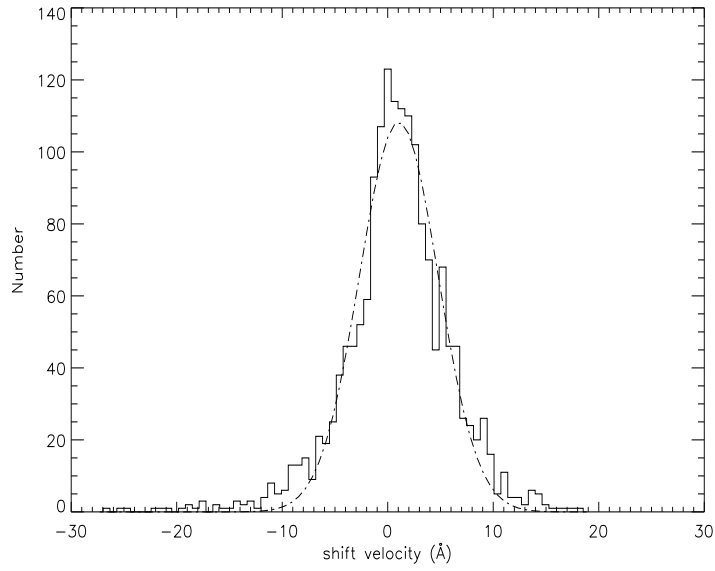


Figure 7. The distributions of shifted velocities of the selected 1672 AGN with standard gaussian broad H α . Thin line represents the histogram of the shift velocities, thick dot-dashed line represents the fitted results by a gaussian function.